



LAWRENCE
LIVERMORE
NATIONAL
LABORATORY

Detecting fiducials affected by Trombone delay in ARC and the main laser alignment at the National Ignition Facility

A. A. Awwal, E. Bliss, V. Miller Kamm, R. R. Leach, R. Roberts, M. C. Rushford, R. Lowe Webb, K. Wilhelmsen

August 5, 2015

SPIE Optics + Photonics
San Diego, CA, United States
August 9, 2015 through August 13, 2015

Disclaimer

This document was prepared as an account of work sponsored by an agency of the United States government. Neither the United States government nor Lawrence Livermore National Security, LLC, nor any of their employees makes any warranty, expressed or implied, or assumes any legal liability or responsibility for the accuracy, completeness, or usefulness of any information, apparatus, product, or process disclosed, or represents that its use would not infringe privately owned rights. Reference herein to any specific commercial product, process, or service by trade name, trademark, manufacturer, or otherwise does not necessarily constitute or imply its endorsement, recommendation, or favoring by the United States government or Lawrence Livermore National Security, LLC. The views and opinions of authors expressed herein do not necessarily state or reflect those of the United States government or Lawrence Livermore National Security, LLC, and shall not be used for advertising or product endorsement purposes.

Detecting fiducials affected by Trombone delay in ARC and the main laser alignment at the National Ignition Facility

Abdul A. S. Awwal*, Erlan S. Bliss, Victoria Miller Kamm, Richard R. Leach Jr., Randy Roberts, Michael C. Rushford, Roger Lowe-Webb, and Karl Wilhelmsen
Lawrence Livermore National Laboratory, Livermore, CA. 94551

ABSTRACT

Four of the 192 beams of the National Ignition Facility (NIF) are currently being diverted into the Advanced Radiographic Capability (ARC) system to generate a sequence of short (1-50 picoseconds) 1053 nm laser pulses. When focused onto high Z wires in vacuum, these pulses create high energy x-ray pulses capable of penetrating the dense, imploding fusion fuel plasma during ignition scale experiments. The transmitted x-rays imaged with x-ray diagnostics can create movie radiographs that are expected to provide unprecedented insight into the implosion dynamics. The resulting images will serve as a diagnostic for tuning the experimental parameters towards successful fusion reactions. Beam delays introduced into the ARC pulses via independent, free-space optical trombones create the desired x-ray image sequence, or movie. However, these beam delays cause optical distortion of various alignment fiducials viewed by alignment sensors in the NIF and ARC beamlines. This work describes how the position of circular alignment fiducials is estimated in the presence of distortion.

Keywords: Optical alignment, pattern recognition, laser alignment, image processing, correlation, matched filtering, position detection, template matching, matched filter, image processing and analysis, high power laser.

1. INTRODUCTION

The Advanced radiographic capability (ARC) is a new diagnostic system for advancing the science of laser-based fusion, which is being developed at the National Ignition Facility (NIF) at the Lawrence Livermore National Laboratory (LLNL). One of the goals of NIF is to create fusion ignition and energy gain in a laboratory setting, which can lead to an almost limitless supply of safe, carbon-free, electricity¹. In 2014, many of the 191 NIF target experiments were designed to advance the path to ignition/discover the perfect operating condition²⁻⁴. In May the NIF average target shot rate was 7.6 shots per week. The total FY15 target shot number is now up to 230 (75% of the 300 shot goal). While with each of the ignition experiments more experimental data is obtained to fine tune and/or advance the physics via computational models of ignition, finer data slices in the spatio-temporal domain are expected to provide an unprecedented view of the reaction dynamics at each time stamp and at different viewing angles of the ignition experiments. The backlighting by the ARC beams⁵ will generate a spatio-temporal history of target evolution, as shown in Fig. 1, during the critical phases of the fusion reaction at the center of the target chamber and thus give NIF scientists a new, powerful tool for optimizing the pathway to ignition.

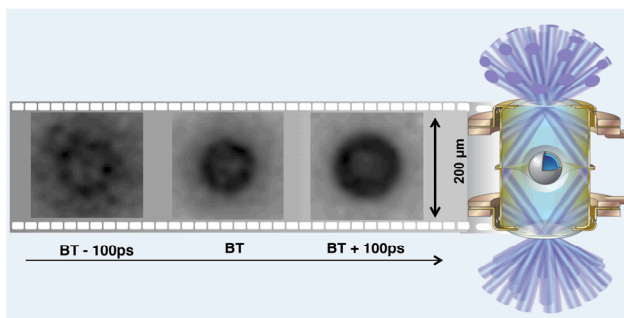


Fig. 1. An ARC backlighting 3 frame simulated radiograph movie at “bang time” (maximum target response).

*awwall@llnl.gov

The ARC system as shown in Fig. 2 uses four of the 192 beams of the National Ignition Facility (NIF) to generate a sequence of short (1-50 picoseconds) petawatt laser pulses (10^{15} watts). The normal path of these beams is shown in gray. When used for ARC, these beams are diverted downward in the target bay to the ARC compressor vessels and then enter the target chamber on the paths indicated in red. Each ARC aperture uses a split-beam arrangement due to space limitations in NIF and the size-limit of fabricating the most advanced diffraction gratings. The split beam architecture causes challenges in the alignment of some of the laser beam fiducials⁷. For backlighting, 8 wires of 30 μm diameter are placed around a target to convert ARC's 1053 nm pulses into high energy x-rays in the range of 50 – 100 Kev, an energy that is capable of penetrating the imploding fuel plasma during ignition scale experiments. The transmitted x-rays imaged with x-ray diagnostics will produce up to eight radiographs that will be captured by gated imaging cameras. The pulses are delayed with respect to each other in a staggered fashion via independent, free-space optical trombones in PABTS (preamplifier beam transport system) as depicted in Fig. 3.

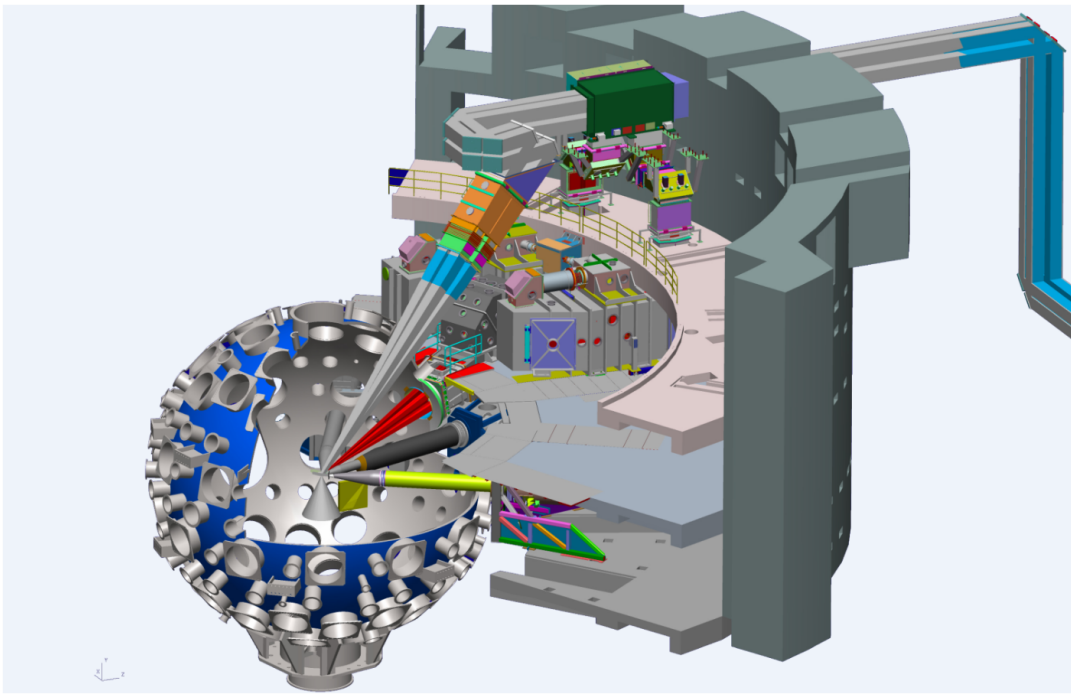
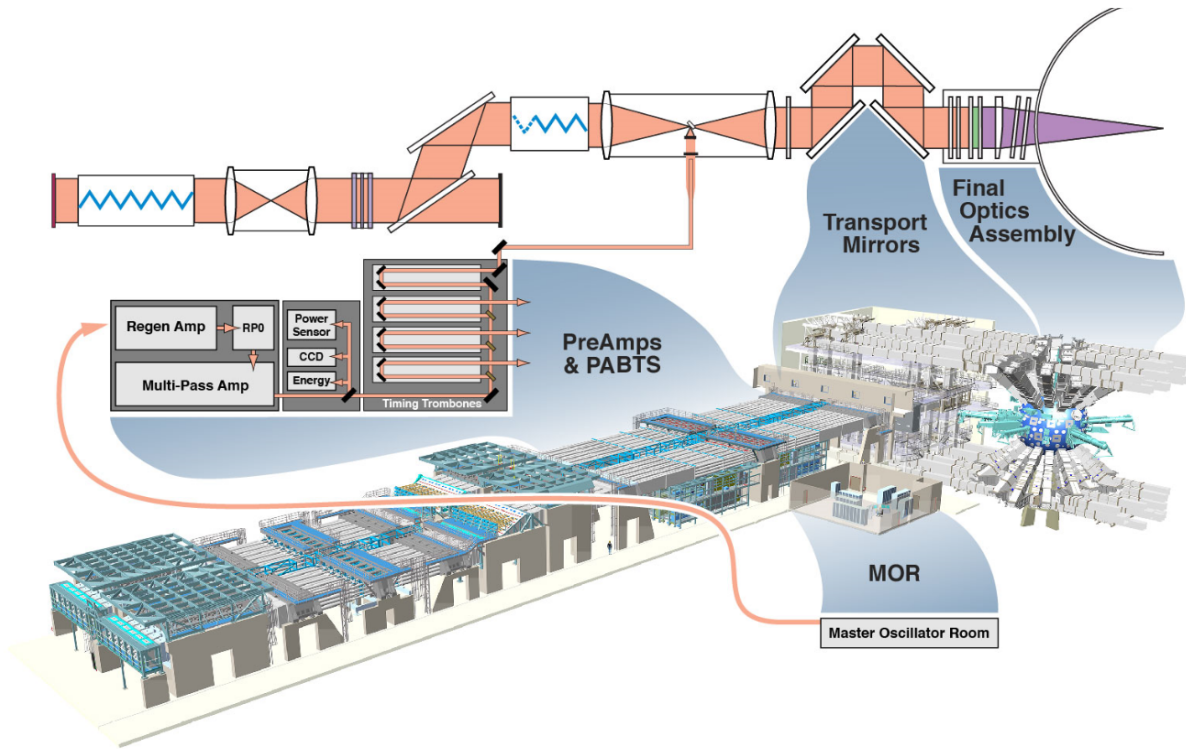


Figure 2. The ARC beam path shown in red and main laser beam when not used in ARC in grey.

The trombone-induced beam-delays create the 8-frame backlit x-ray movie of the implosion of the target, and placement of the x-ray source wires at different locations produces different spatial points of view of the target implosion. However, the beam delay necessary for creating a movie effect also causes optical distortion in the images of various beam alignment fiducials used in both in the main laser and the ARC system. This paper describes how these alignment fiducials are detected and their positions estimated in the presence of challenging distortion.

NIF is a very large 192 beam laser. Each of the 300m long beams is aligned using a series of automated alignment (AA) loops. The loops use efficient automated image processing algorithms to identify fiducials imprinted on the beams, and the AA control system is able to align the main laser in 30 minutes⁷. Because NIF uses database driven software control that allows the instructions for processing each beamline to be independently controlled, automatic alignment of the ARC beams incorporates additional image processing algorithms have been developed to align the ARC laser^{8,9} system. This enables the alignment system to control the modified beam paths of ARC and to accurately process the defocused fiducial images described above.



15MLS/cld - 2012-034415a2 MOR+LB+TB L0 L8 L9 L10

Figure 3. Trombone used for the ARC beams

In this paper, we describe a method of detecting the beam fiducials as seen by the output sensor package (OSP) camera in the main laser beams and also for ARC beams. We first describe the basic algorithm with no distortion as shown in Fig. 4(a). Then, we describe how the fiducials are detected in the presence of the trombone-induced distortions as depicted in Fig. 4(b).

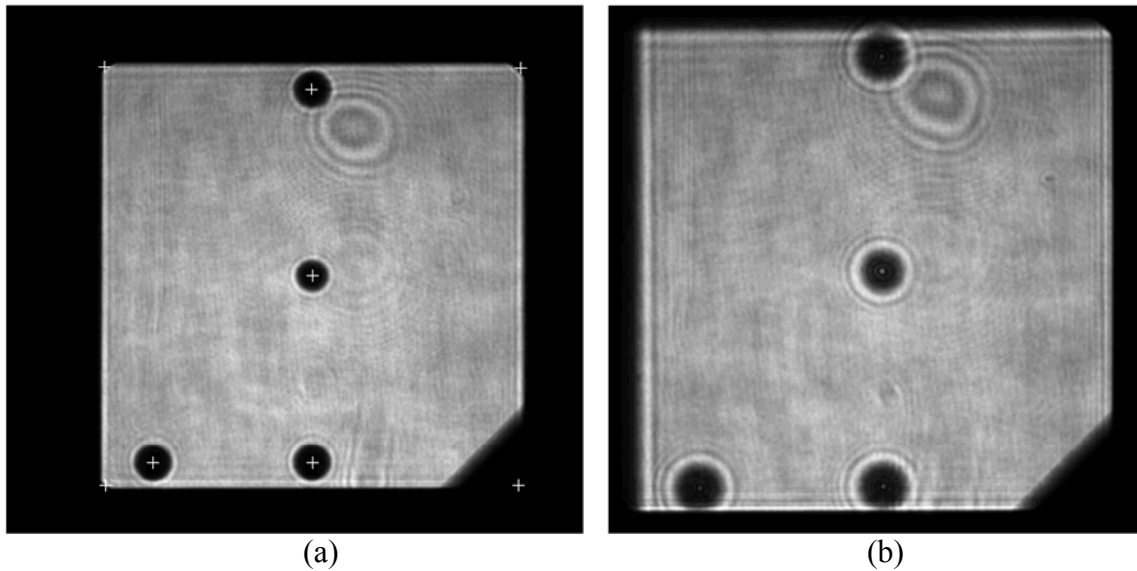


Figure 4. OSP image (a) without trombone delay and (b) with trombone delay

2. MATHEMATICAL BACKGROUND

Undistorted images are detected by a classical matched filter. However, for distorted trombone images, the matched filter provides only the first estimate. Alignment “mask” (circular) dot images illustrated in Fig 4(a) are viewed near focus for NIF beams. ARC beams require different timing, adjusted with trombone delay between relay telescopes, making the mask image out of focus as in Fig. 4(b). Edge diffraction makes some dots appear with flattened edges. For extreme defocus, Poisson spots appear at the center of these dots. As a result of these various forms of distortion to the circular shape, the first, matched filter estimate is refined based on successive approximation by repeated matched filtering or techniques based on physical optics considerations. The complex matched filter (CMF) is well known for its position detection capability where the position of the object can be derived from the position of the correlation peak. A CMF^{10,11} is defined by assuming that the Fourier transform of the object function $f(x,y)$ is denoted by:

$$F(U_x, U_y) = |F(U_x, U_y)| \exp(j\Phi(U_x, U_y)) \quad (1)$$

The CMF for detecting the function $f(x,y)$ and its location, is given by the complex conjugate of the Fourier spectrum $F(U_x, U_y)$ as denoted in Eq. 2,

$$H_{CMF}(U_x, U_y) = F^*(U_x, U_y) = |F(U_x, U_y)| \exp(-j\Phi(U_x, U_y)) \quad (2)$$

The shape of correlation and the discrimination capability of CMF can be enhanced by using the edge of the to-be-detected images¹². The position of the object is related to the position of the cross correlation, autocorrelation, and the template using Eqs. 3(a-b).

$$X_{\text{pos}} = X_{\text{cross}} - X_{\text{auto}} + X_c \quad (3a)$$

$$Y_{\text{pos}} = Y_{\text{cross}} - Y_{\text{auto}} + Y_c \quad (3b)$$

The value of $(x_{\text{pos}}, y_{\text{pos}})$ is the to-be-determined position of the pattern in the image plane. The value of $(x_{\text{auto}}, y_{\text{auto}})$ is the position of the template autocorrelation peaks and the value of $(x_{\text{cross}}, y_{\text{cross}})$ is the position of the cross correlation peak. The position of the cross-correlation peak is estimated using a polynomial fit of second order to the correlation peak. The center of the template, (x_c, y_c) is calculated offline or on the fly for a regular object such as a circle as the case is here. The $(x_{\text{auto}}, y_{\text{auto}})$ are calculated off-line. By aligning the center of x_c and y_c with x_{auto} and y_{auto} , the position of the circle fiducials will coincide with those of the correlation peak. However, for practical reason it is better to use the whole Eq. (3) without making any assumption and use the dynamic values. Figure 5(a) shows the correlation plane output for detecting the smaller inner circle, which is shown as the highest peak. Note that the Fig. 4 shows the four circles arranged as a left sided-L. By threshold detection of the highest single or triple peak, and by successive zeroing out the position, we are able to detect all four of the peaks. Further refinement by polynomial approximation results in subpixel accuracy.

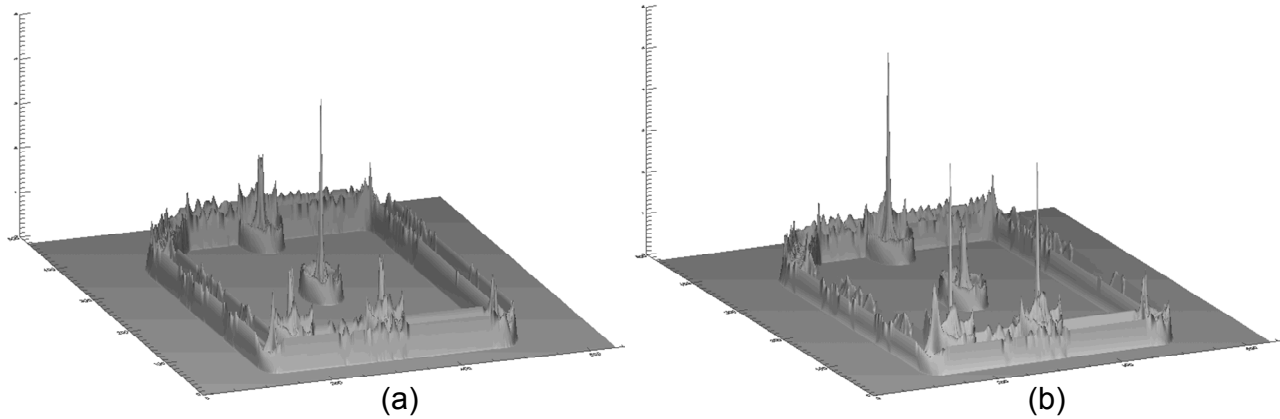


Figure 5. (a) Correlation plane output for center fiducial and (b) correlation peaks for the off-center fiducials.

3. THE BASIC ALGORITHM

The main laser input sensor package (ISP) beam mask is imaged in the OSP, as shown in Fig. 4(a). While the center fiducial defines the beam center, the orientation of off-center fiducials allows one to identify a specific beam within a quad and determine the beam rotation angle. For beam alignment, it is essential to detect the center fiducial, which allows the control loop to perform alignment operation. In the absence of trombone delay, the loop exhibits a normal mask pattern as shown in Fig. 4(a). The basic algorithm for detecting the circles in a normal image with no distortion is outlined below and illustrated in Fig. 6.

The steps for detecting the fiducials in a normal mask image are as follows:

1. *Image is smoothed, binarized, and inverted.*
2. *The circular blobs are analyzed and sorted according to area. The approximate radius of each type of circle is determined by segmenting each area and performing a search on the subimage by changing search radius for best match¹³. Thus we obtain radii r_1 and r_2 . Note that the central circle is identified as being the smallest one.*
3. *An edge-detection is performed on the binarized image before each search and subsequent correlation.*
4. *Next the whole edge image is correlated with circles with two different radii.*
 - a. *First the location of the center circle is determined using the smaller radius.*
 - b. *Then the remaining four circle positions are detected using higher radius*
5. *An integrity check of approximate position is performed to ensure that the center circle is near the center of the image. A spacing test is performed amongst all four circles, to ensure they satisfy the horizontal and vertical inter-spot spacing within a nominal tolerance.*

These steps are explained in Fig. 6 as well as Table I, which contains a typical output log from the algorithm.

Step 1: Consider an OSP image as shown in Fig. 6(a). After smoothing the image in Fig.6(b) results. Inverting the image produces 4 white blobs. The output in 6(c) is the end result of step 1.

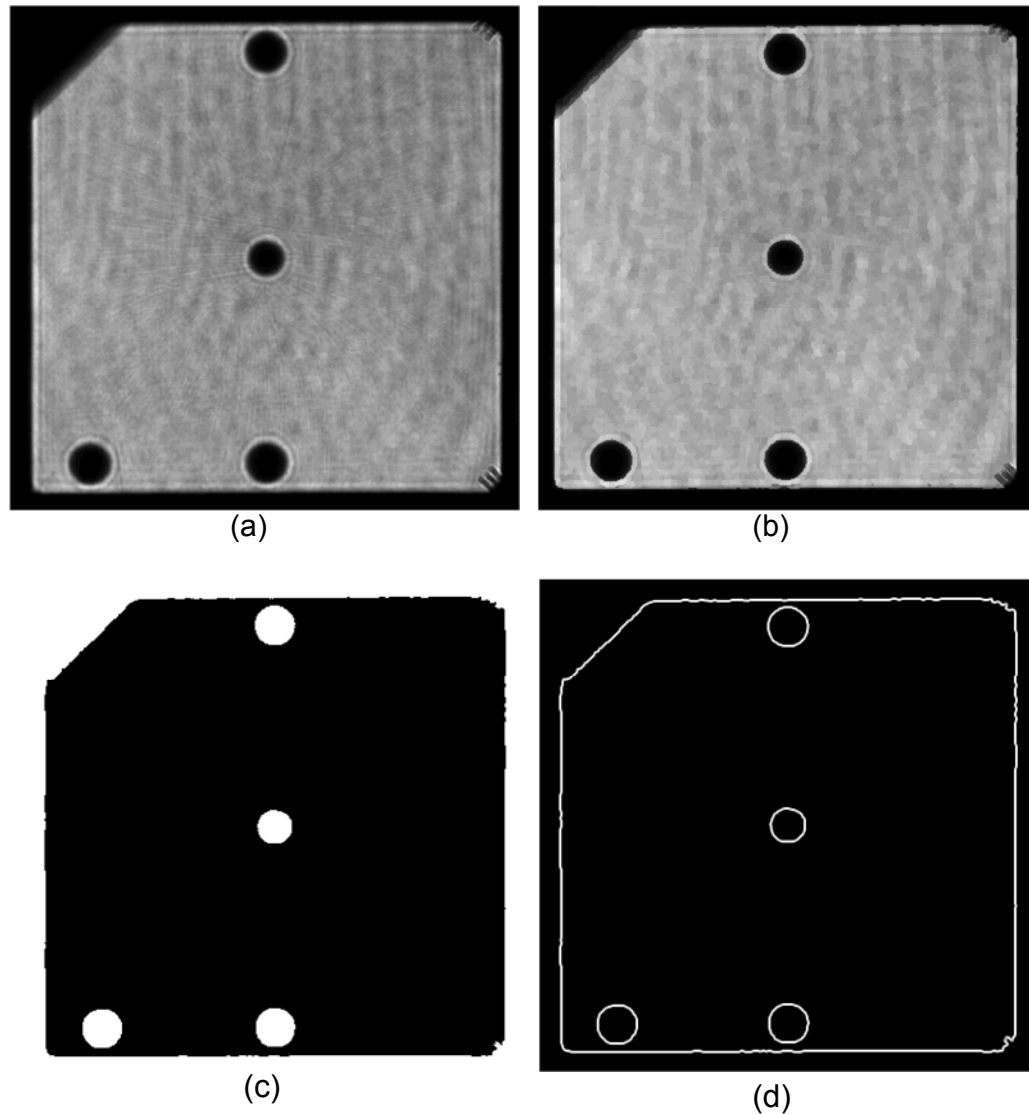


Figure 6. (a) Original OSP image (b) Smoothed image (c) Inverted image (d) Edge image

Steps 2 & 3: The image type as shown 6(c) is analyzed for the blob sizes. A typical output shown in Table I shows three different blob sizes were found with 782, 593, and 813 areas in pixels. Obviously, the smaller size corresponds to the center circle. Note from the log in Table I that an approximate center of each of the blobs is also calculated. For each blob position size a subimage is formed around the approximate center, and a radius search is executed by taking an edge of the subimage and performing correlation with varying radii. In this case, there are mainly two sizes, a small circle at the center at (312, 261) and a bigger circle at the outside at (311.5, 94.5), these two blob sizes are analyzed to match to two nominal sizes. The step 2 ensures that when beam-to-beam variations exist, they do not affect the accuracy of the position, since the template for each of the individual images is estimated dynamically¹².

Steps 4(a-b): The whole image is correlated with the small radius, which results in an output shown in Fig. 5(a). Then the larger radius, r2 is used to correlate with the image in Fig. 6(d), which results in output shown in Fig. 5(b). Note that in step 2, we only chose one of the three off-center circles and made the assumption that all three off-center circles have the same radius. For a standard ISP mask image without any trombone delay this is a valid assumption, which is verified by the relatively close magnitude levels of these three correlation peaks as shown in Fig. 5(b). Note that after choosing the highest correlation peak, it is normalized by the maximum correlation peak to 1. The other peaks are also scaled with

respect to the highest peak. In this case, the second peak is 74% of the first peak and third peak is 54%. A nominal threshold of 50% is used, so that in this case all three peaks are detected.

Step 5: An integrity check ensures that the circle is indeed the smallest and is located near the center of the image. In this step various inter-spot distances are tested and verified. For example, the three large spots have a 154 pixel x-distance and 364 pixel y-separation within a tolerance of 70 pixels. This step is important because as can be seen from Fig. 6(d), the almost square perimeter of the beam may give rise to spurious peaks matching partially to the center circle radius as shown in Fig. 5. There are two protections against spurious peak selection. First, the detection threshold is expected to be at least 50% of the peak value, so that peaks below this level are ignored. The second protection is the spacing and absolute position test. When the image quality deteriorates, the threshold may not detect all three large spots, and the algorithm may fail. If any specific beam is consistently failing due to lower quality, we can externally supply a reduced detection threshold for that particular beam. The above general algorithm has been applied successfully in other NIF alignment systems such as PAM (preamplifier module) alignment¹⁴ on images containing both circle and square fiducials as well as in PSS (programmable spacial shaping) for finding blocker size and positions¹⁵.

Table I. Output log from a main laser trombone image processing algorithm

Output from Step 2:

Feature sizes of interest 782 593 813
Found 3 spots in the valid range [250, 1400]
For Blob 782: x = 311.50, y = 94.50
For Blob 593: x = 312.00, y = 261.00
For Blob 813: x = 312.00, y = 427.50
Searching for small (inner) circle at 312.00, 261.00
Interesting spots 3
Insufficient spots detected.....
Searching for big circles at 311.50, 94.50
Small radius = 13.5 Big radius = 16.0

Output of Steps 4 to 7:

Looking for the inner circles with radius 13.5
xpos, ypos = 311.81, 260.94 corr = 1.00
Found 1 inner circle spot

Looking for the inner big circles with radius 16.0
xpos, ypos = 313.00, 94.19 corr = 1.00
xpos, ypos = 310.40, 427.70 corr = 0.95
xpos, ypos = 454.94, 95.96 corr = 0.54
Found 3 big circles spots

Steps after Step 7 due to Trombone Effects

Detecting presence of Poisson spots...
No Poisson spot detected in 1 locations...
No Poisson spot detected in 3 locations...
Refining the positions...

Step 8 spacing test

Selected 1 center spot after spacing test
Center spot passed tight ROI test
Found 3 big circles before spacing test
Testing 3 spots for pixel x-spacing 154 and y-spacing 364
The current tolerance is 70 pixels

Selected 3 circle spots after spacing test
Center passes relative position test...

4. ALGORITHM IMPROVEMENTS

Next, we describe algorithm modifications to detect the fiducials in the presence of trombone-induced distortions. As beam delay is increased, evidence of defocus appears. During the early phase of NIF construction in 2004, four initial NIF beams were subjected to trombone delay. The resulting distorted circular fiducial pattern was classified by the size of the central circle, which was identified as small, medium or large. Then an improved position was obtained by searching over a range centered around the nominal radius of that class¹⁶. This is the first improvement for processing out of focus images of alignment fiducials.

Further modifications are required for steps 2 to 4. As shown in Fig. 7(c), image noise can cause the central fiducial edges to show up as two small objects. By modifying the binarization threshold towards a higher value the problem is overcome and we get the image seen in Fig. 8(a). An additional effect is seen in Fig. 7(a). Defocus caused by trombone delay leads to diffraction rings forming around each spot and diffraction lines at the beam boundaries. Figures 7(c) and 8(a) illustrate that the interaction between these two patterns results in a noncircular shape of the edge detected fiducial spots compared to a similar image shown in Fig. 6(d).

The output of step 4(b) is shown in Fig. 8(b) where a well-defined correlation with the small radius spot is detected. However, when the higher radius is correlated with the entire image, only the spot at the top shows a high peak value. The other two spots show a much lower value as shown in Fig. 9(a). This is because when trombone delay defocus is introduced, the assumption that all circles are of same size is no longer valid and leads a peak below threshold of 50%. In this case, the second and third peak may not be detected.

When the other two spots have a lower relative magnitude, the detection threshold is lowered to get an approximate location of the off-center spots. There are two possible scenarios for a defocused spot. It may exhibit a very broad defocus with no well-defined boundary and no strong Poisson or there may be a sharp Poisson spot in the center location.

First a check is made to detect the Poisson spot in small region of interest around the approximate circle location. The maximum value of the Poisson spot must exceed a threshold related to the nearby region, to be detected. If it is found then we approximate the peak location, which becomes the location of the circle. If a Poisson spot is not present, then the subimage around the center location is extracted and a search is conducted to find the right radius for the defocus circle and then the new radius is used to find a better approximation of the circle center. The process is repeated for the other circle fiducials with low correlation peak values. Figure 9(b) demonstrates that this additional processing results in accurate identification of all four fiducials.

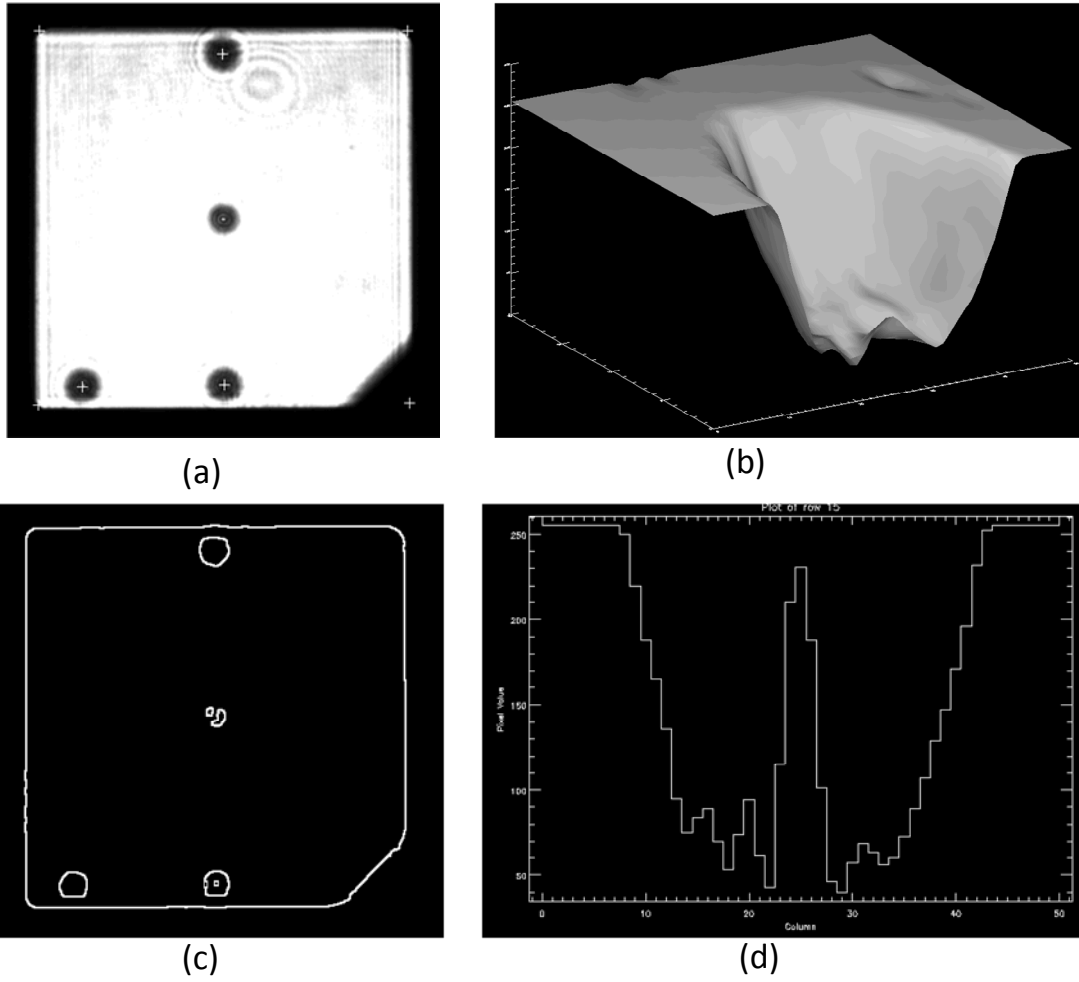


Figure 7. A defocused image with an elevated background level inside the center spot causes the binarized edge image to have two parts. Thus a circle match with the smallest radius fails to locate the center spot, and the basic algorithm fails.

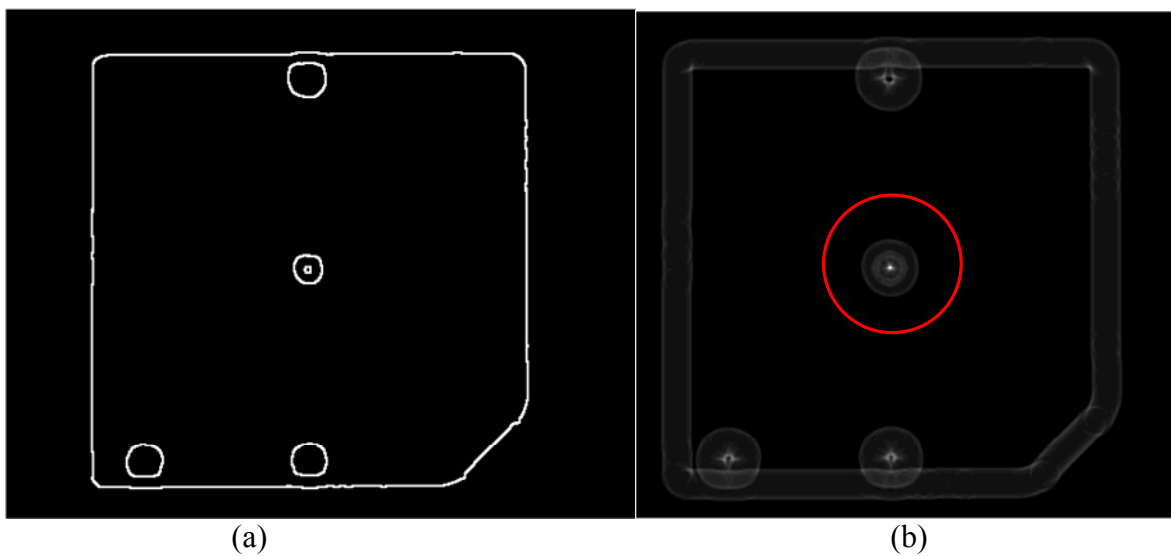


Figure 8. (a) Edge image from a trombone image (b) correlation plane output for small circles at the center

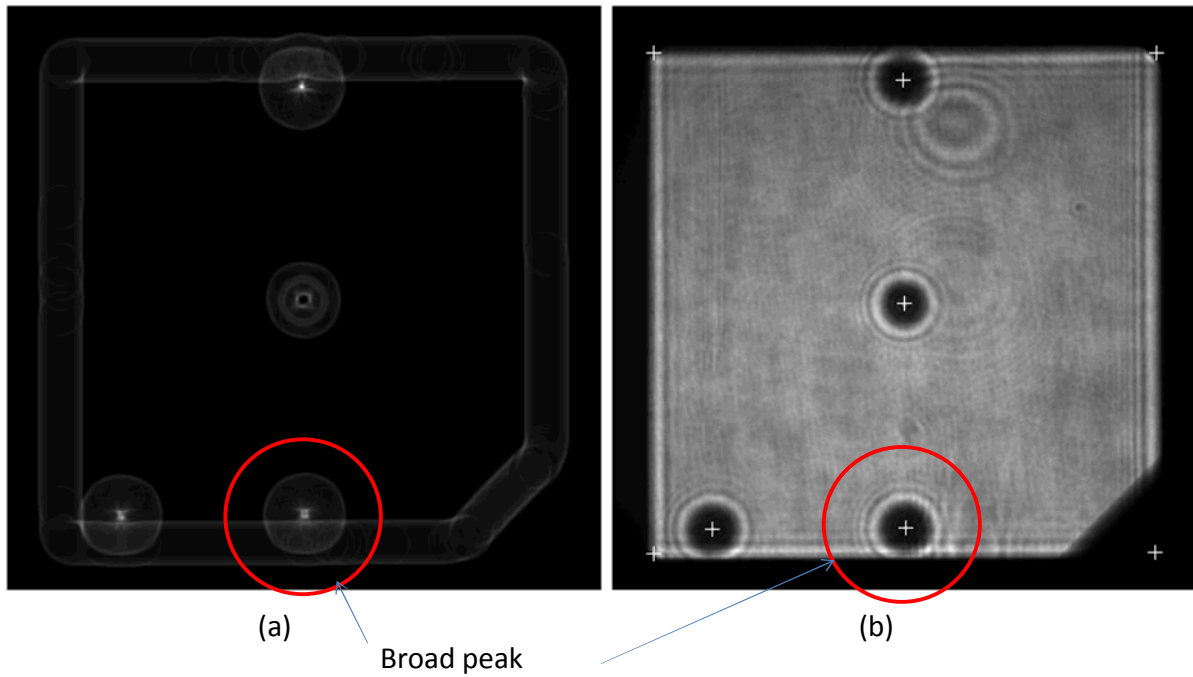


Figure 9. Position detection despite heavy distortion.

For ARC images, the beam is split into two parts, and the center fiducial is divided into two halves. This causes the position of the center to be displaced as seen in Fig. 10 and therefore cannot be used as representing true beam center. Therefore for ARC images, the center image location is recalculated based on the off-center fiducials. Thus any initial detected center spot is overwritten by the average location.

For ARC alignment images obtained after the compressor, the techniques already described are used to determine fiducial spot locations. However, as is evident in Figure 10, propagation through the compressor adds some noise to the beam. This requires adjustment of the image processing parameters to optimize the result.

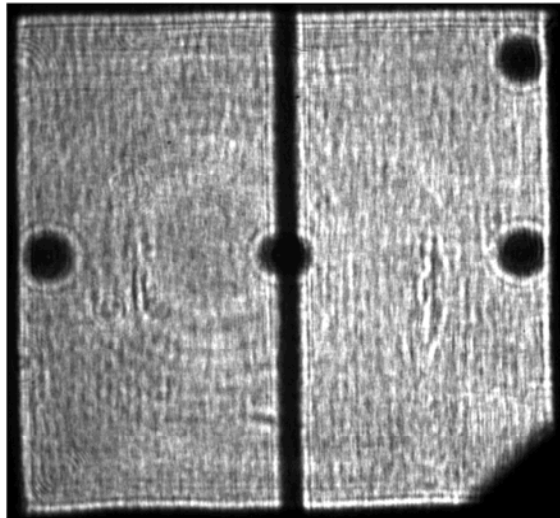


Figure 10. ARC alignment image at the output of the compressor in the target bay

5. CONCLUSION

In this work we discuss automatic alignment algorithms for OSP (output sensor package) images under normal conditions and for images with trombone-induced focus distortion. It is shown that using a recursive process of gradual approximation achieves better position accuracy. Mainly two types of defocused images are processed: images from normal main laser beams and a second type from ARC beams. Separately optimized algorithms are used to process each type. The algorithms are effective in processing images that may be distorted due to trombone effects of varying magnitude.

ACKNOWLEDGEMENT

This work performed under the auspices of the U.S. Department of Energy by Lawrence Livermore National Laboratory under Contract DE-AC52-07NA27344. The paper is released as LLNL-CONF-xxxxx. The authors acknowledge Clayton Dahlen for providing some of the figures and Otto Landen for providing an important reference to ARC.

REFERENCES

- [1] Stolz, C.J., et al., "[The National Ignition Facility: the path to a carbon-free energy future.](#)" *Philos. T. Roy. Soc. A*, v. **370**, 4115-4129 (2012)
- [2] Moses, E. I., et al., "[The National Ignition Campaign: status and progress.](#)" *Nucl. Fusion*, v. **53**, 104020 (2013)
- [3] Hurricane, O.A., et al., "[Fuel gain exceeding unity in an inertially confined fusion implosion.](#)" *Nature*, v. **506**, p.343-+ (2014)
- [4] Lindl, J., et al., "[Review of the National Ignition Campaign 2009-2012.](#)" *Phys. Plasmas*, v. **21**, 020501 (2014)
- [5] R. Tommasini, S. P. Hatchett, D. S. Hey, C. Iglesias, N. Izumi, J. A. Koch, O. L. Landen, A. J. MacKinnon, C. Sorce, J. A. Delettrez, V. Yu. Glebov, T. C. Sangster, and C. Stoeckl, "Development of Compton radiography of inertial confinement fusion implosions," *Physics of Plasmas* 18, 056309 (2011)
- [6] Awwal, A. A. S., Leach, R. R., Roberts, R.S., Karl Wilhelmsen, David McGuigan, Jeff Jarboe, "Detecting objects with partial obstruction at the ARC split beam injector images at the National Ignition Facility," *Proc. SPIE. 9216, Optics and Photonics for Information Processing VIII*, 92160E (2014).
- [7] Burkhart, S.C., E. Bliss, D. Kalantar, R. Lowe-Webb, T. McCarville, D. Nelson, ... K. Wilhelmsen, "National Ignition Facility system alignment," *Applied Optics*, **50**(8), 1136-57 (2011).
- [8] Leach, R.R., Abdul Awwal, Erlan Bliss, Randy Roberts, Michael Rushford, Karl Wilhelmsen, Thomas Zobrist, "Analysis of the confluence of three patterns using the Centering and Pointing System (CAPS) images for the Advanced Radiographic Capability (ARC) at the National Ignition Facility," *Proc. SPIE. 9216, Optics and Photonics for Information Processing VIII*, 92161Q (2014).
- [9] Roberts, R.S., Erlan S. Bliss, Michael C. Rushford, John M. Halpin, Abdul A. S. Awwal, Richard R. Leach, "Image analysis algorithms for the advanced radiographic capability (ARC) grating tilt sensor at the National Ignition Facility," *Proc. SPIE. 9216, Optics and Photonics for Information Processing VIII*, 92160B, 2014.
- [10] Karim M. A., and A. A. S. Awwal, [Optical Computing: An Introduction], John Wiley, New York, NY (1992).
- [11] Awwal, A. A. S., M. A. Karim, and S. R. Jahan, "Improved Correlation Discrimination Using an Amplitude-modulated Phase-Only Filter," *Applied Optics*, **29**, 233-236 (1990).
- [12] Awwal, A. A. S., "What can we learn from the shape of a correlation peak for position estimation?," *Applied Optics*, **49**, B41-B50 (2010).
- [13] Awwal, A. A. S., "Automatic identification of the templates in matched filtering," *Proc. of SPIE Vol. 5556, Photonic Devices and Algorithms for Computing VI*, 102-109, 2004.
- [14] Awwal, A. A. S., "Multi-object feature detection and error correction for NIF automatic optical alignment" in *Photonic Devices and Algorithms for Computing VIII*, edited by K. Iftekharuddin and A. A. S. Awwal, *Proc. of SPIE Vol. 6310*, 63100Q (2006).
- [15] Awwal, A. A. S., et al., "Image processing and control of a programmable spatial light modulator for spatial beam shaping," *SPIE Proceedings Volume 8602: High Power Lasers for Fusion Research II* (2013)
- [16] Awwal, A. A. S., James V. Candy, Chris A. Haynam, Clifford C. Widmayer, Erlan S. Bliss, Scott C. Burkhart, "Accurate position sensing of defocused beams using simulated beam templates" *Proc. SPIE. 5556*, 233 (2004).